AIAA-90-1213-CP

VIBRATION LOCALIZATION BY DISORDER IN ASSEMBLIES OF MONO-COUPLED, MULTI-MODE COMPONENT SYSTEMS*

*Philip D. Cha,** Christophe Pierre†*

Department of Mechanical Engineering and Applied Mechanics
The University of Michigan
Ann Arbor, Michigan

1. ABSTRACT

Disorder in nominally periodic engineering structures results in the localization of the mode shapes to small geometric regions and in the attenuation of waves, even in the passbands of the corresponding perfectly periodic system. This paper investigates, via probabilistic methods, the transmission of steady-state harmonic vibration from a local source of excitation in nearly periodic assemblies of mono-coupled, multi-component mode substructures. A transfer matrix formulation is used to derive analytical expressions for the localization factor (the rate of exponential decay of the vibration amplitude) in the limiting cases of strong and weak modal coupling. The degree of localization is shown to increase with the ratio of disorder strength to modal coupling. The increase is nearly parabolic for small values of this ratio, and logarithmic for large values. Furthermore, the localization factor increases very rapidly with the passband number. Typically, the transition from weak to strong localization occurs from one passband to the next, and severe vibration confinement is unavoidable at high frequencies, even for very small disorder.

2. INTRODUCTION

The dynamic analysis of repetitive engineering structures is greatly simplified by assuming perfect periodicity. However, unavoidable manufacturing and material tolerances destroy this mathematical idealization. Typical examples of often-assumed-periodic structures are bladed disk assemblies and large space structures.

Unfortunately for the designer and analyst confronted with repetitive structures, slight disruption in their periodicity may alter drastically the dynamic response from the assumed-periodic predictions. For example, under conditions of weak internal coupling, the extended mode shapes of the ideally periodic structure become localized to a small geometric region when small disorder (or mistuning) is introduced. This phenomenon, known as normal mode localization, was first evidenced by Hodges[1] in the field of structural dynamics (although the phenomenon has excited the interest of solid state physicists for many years).

The motivation for studying localization is threefold. First, the occurrence of localization may severely reduce the effectiveness of structural models, associated control schemes, and identification techniques that assume perfect periodicity. For example, a control strategy based upon the erroneous extended modes of a perfectly periodic structure would be unpredictable. Second, localized vibrations increase amplitudes and stresses locally and may result in severe damage. For instance, single-blade failure in turbomachinery rotors is a plausible result of blade mistuning. Third, when localization occurs, irregularities exhibit a damping-like effect that could be used as a passive control of vibration transmission. This has applications in flexible and lightly damped structures such as truss beams in space. However, although disorder and dissipation both result in an exponential spatial decay of the amplitude, the localization and damping mechanisms are intrinsically distinct: for localization the vibrational energy is *confined* near the source of excitation by disorder (through multiple scatterings), while for damping the energy is *dissipated* as it propagates.

Research on localization in structural dynamics has been limited mostly to *deterministic* analyses of the free modes of disordered one-dimensional structures. Here we cite several representative studies. Pierre and Dowell[2] investigated mode localization by perturbation methods for a chain of coupled oscillators. Valero and Bendiksen[3] evidenced strongly localized modes for shrouded blades of jet engine rotors. Other works by Bendiksen[4], Cornwell and Bendiksen[5], and Wei and Pierre[6] examined the occurrence of mode localization in mistuned cyclic periodic structures such as large space reflectors and blade assemblies. Pierre and Cha[7] tackled localization analytically in assemblies of *multi-mode* component systems and showed that confinement effects increase rapidly with frequency. This result was confirmed recently by Cornwell and Bendiksen[8], who examined a similar (but cyclic) structure by defining a deterministic localization length scale.

Considerably fewer *probabilistic* studies of localization have been conducted. Hodges and Woodhouse[9] formulated a statistical treatment of the transmission of harmonic forced vibrations from a local source of excitation. They applied the work of Herbert and Jones[10] to calculate localization factors (the exponential spatial decay rate of the amplitude) for a stretched string with irregularly spaced masses attached. Although they did not study localization effects systematically in terms of frequency or system parameters, their work exhibited two types of localization—*weak* and *strong*—depending on the magnitude of internal coupling in the structure. Recently, Kissel[11,12] chose the wave description of Ishii[13] to calculate localization factors for several infinite one-dimensional structures. He studied systematically the dependence of the localization factor inside the passbands on the frequency in the limiting case of weak disorder. However, the models he chose did not allow him to vary the relative magnitudes of internal coupling and disorder, thereby restricting his findings to *weak* localization effects. Recently, Pierre[14] developed stochastic perturbation methods based upon modal or wave formulations to calculate localization factors in terms of frequency, coupling, and disorder strength. He evidenced both *weak* and *strong* localization regimes and established their relevance to structural dynamics applications. His study, however, was restricted to chains of coupled oscillators, i.e., assemblies of *single-mode* subsystems.

This paper investigates weak and strong confinement effects of random disorder in assemblies of *multi-mode* component systems. Special attention is paid to the dependence of degree of localization on frequency, both inside a passband (or, equivalently, for a group of modes) and from passband to passband. The transmission of steady state vibration and the propagation of incident waves from a local excitation source is studied by probabilistic techniques that are reviewed in section 3. The frequency stopbands and passbands of the ordered assembly are discussed in section 4. Statistical perturbative techniques are used to derive analytical expressions for the localization factors in the two limiting cases of strong and weak modal coupling in section 5, and the analytical results are verified by Monte Carlo simulations in section 6. In section 7, the

* This work is supported by National Science Foundation Grant No. MSM-8700820, Dynamic Systems and Control Program. Dr. Elbert L. Marsh is the grant monitor.

** Currently, Staff Research Engineer, Ford Motor Company.

† Member AIAA, ASME. Assistant Professor

dependence of the localization factor on disorder strength, modal coupling, and passband number (frequency) is investigated. Finally, the relevance of the localization phenomenon to structural dynamics applications is illustrated by an example.

The contributions of the present study are twofold. First, analytical results of general significance to the theory of localization in engineering structures are presented. For example, the dependence of localization effects on frequency and disorder strength is thoroughly examined for both weak and strong localization regimes. Second, it is shown that, for assemblies of multi-mode subsystems, confinement effects at high frequencies (in the higher groups of modes) are severe, and unavoidable even if the internal coupling is very large and the disorder very small. This has important consequences for many structural dynamics applications.

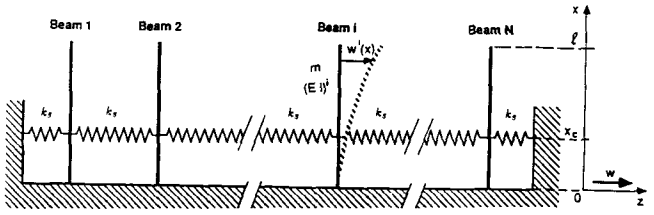

Fig. 1 Assembly of coupled, component systems (cantilevered beams).

3. CALCULATION OF LOCALIZATION FACTORS

3.1 Equations of Motion

Consider an undamped assembly of N, mono-coupled, one-dimensional, almost identical component systems (see Fig. 1). Each subsystem is coupled to its nearest neighbors through linear springs of stiffness k_s located at $x = x_c$ along each component structure. To study vibration transmission, the system is excited at its left end by a simple harmonic force of frequency, ω, and the steady state response of the right-end component is examined. Applying component mode analysis[15], the nominal component system is represented by its modal representation, $(\lambda_p, \phi_p(x))_{p=1,\ldots,M}$, where M is the number of component modes, λ_p the pth eigenvalue (the square of the pth natural frequency), and $\phi_p(x)$ the corresponding mode shape. In the presence of disorder, the modes of the ith (uncoupled) component system are slightly perturbed, becoming

$$\begin{cases} \lambda_p^i = \lambda_p(1 + d\lambda_p^i), & p = 1,\ldots,M \quad ,i = 1,\ldots,N \\ \phi_p^i(x) = \phi_p(x)(1 + d\phi_p^i(x)), & p = 1,\ldots,M \quad ,i = 1,\ldots,N\,, \end{cases} \tag{1}$$

where p denotes the component mode number, and i the component system number.

For simplicity, we assume no component mode shape perturbation due to disorder, as well as constant modal mistuning; thus, $\phi_p^i(x) \equiv \phi_p(x)$ and $d\lambda_p^i \equiv d\lambda^i$. Furthermore, denoting the pth modal mass of the ith component system by M_p^i, we choose them to be identical for all component systems* and all component modes;† thus, $M_p^i \equiv \mathcal{M}$. These assumptions allow for all the important localization effects to be captured in a relatively straightforward analysis. For harmonic motion the deflection amplitude of the ith component system is expanded as

$$w^i(x) = \sum_{p=1}^{M} \phi_p(x)\,\eta_p^i \qquad ,i = 1,\ldots,N \quad , \tag{2}$$

where η_p^i is the pth normal coordinate amplitude for the ith subsystem. Applying Lagrange's equations gives (see reference 7 for the detailed derivation)

$$\left([K] - \omega^2[I]\right) \begin{bmatrix} \underline{\eta}^1 \\ \underline{\eta}^2 \\ \vdots \\ \underline{\eta}^i \\ \vdots \\ \underline{\eta}^N \end{bmatrix} = \begin{bmatrix} \frac{F}{\mathcal{M}}\underline{\phi}_f \\ \underline{0} \\ \vdots \\ \underline{0} \\ \vdots \\ \underline{0} \end{bmatrix}, \tag{3}$$

where $\underline{\eta}^i$ is the M-vector of amplitudes for the ith component system, $\underline{\phi}_f = [\ldots, \phi_p(x_f), \ldots]^T$ the M-vector of modal deflections at the forcing location, F the forcing amplitude, $\mathcal{M}$ the modal mass, $[I]$ the $NMxNM$ identity matrix, and $[K]$ the $NMxNM$ block tridiagonal matrix

$$[K] = \begin{bmatrix} \ddots & \ddots & [0] & \ldots & [0] \\ \ddots & \ddots & \ddots & \ddots & \vdots \\ [0] & -R[A] & [D^i] & -R[A] & [0] \\ \vdots & \ddots & \ddots & \ddots & \ddots \\ [0] & \ldots & [0] & \ddots & \ddots \end{bmatrix}, \tag{4}$$

where

$$[A] = \underline{\phi}_c\,\underline{\phi}_c^T\,, \qquad [D^i] = [\Lambda](1 + d\lambda^i) + 2R\,\underline{\phi}_c\,\underline{\phi}_c^T\,. \tag{5}$$

$R = k_s/\mathcal{M}$ can be regarded as a coupling frequency squared, $[\Lambda] = [\mathrm{diag}(\lambda_p)]$ is the MxM diagonal matrix of the eigenvalues of the nominal subsystem, and $\underline{\phi}_c$ is the M-vector of modal deflections at the constraint location, x_c.

While the theoretical results derived in this paper hold for the generic assembly of component systems introduced above, all the numerical calculations are performed on an assembly of clamped-free Euler-Bernoulli beams (see Fig. 1). We assume there is no domain perturbation and that disorder originates from discrepancies among the flexural rigidities $(EI)^i$ of the beams. Thus, the modal mass is $\mathcal{M} = ml$, the component modes, $\phi_p(x)$, are the modes of a clamped-free beam (see the expression in reference 7), and the equations of motion (3) are divided by EI/ml^4 to introduce the dimensionless parameters $\overline{R} = k_s/(EI/l^3)$, $\overline{\lambda}_p = \lambda_p/(EI/ml^4)$, $\overline{\omega}^2 = \omega^2/(EI/ml^4)$, and $\overline{F} = F/(EI/l^3)$, where EI is the flexural rigidity of the nominal beam.

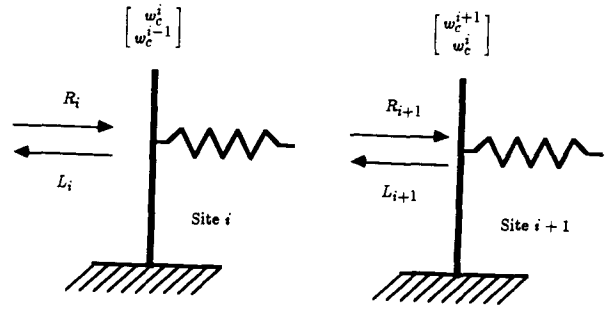

Fig. 2 Site representation for wave formulation.

3.2 Wave Formulation

We choose a traveling wave perspective to study the transmission of vibration and to calculate the associated spatial amplitude decay. Since the nearly periodic assembly shown in Fig. 1 is mono-coupled, it carries a single pair of waves and thus can be modeled by 2x2 transfer matrices. We choose the ith bay to consist of the ith component system and the coupling spring to its right, as shown in Fig. 2. Defining the state vector of normal coordinates at the ith site by $[\underline{\eta}^i, \underline{\eta}^{i-1}]^T$, the $2Mx2M$ normal coordinate transfer matrix that relates the states at adjacent sites is given by

* This is the case if perturbation methods for the eigenvalue problem are used to obtain the modes of the mistuned component systems, as these methods conserve the generalized masses.

† This is the case if the modes are normalized consistently.

$$\begin{bmatrix} [A] & [0] \\ [0] & [A] \end{bmatrix} \begin{bmatrix} \underline{\eta}^{i+1} \\ \underline{\eta}^{i} \end{bmatrix} = \begin{bmatrix} [B^i] & -[A] \\ [A] & [0] \end{bmatrix} \begin{bmatrix} \underline{\eta}^{i} \\ \underline{\eta}^{i-1} \end{bmatrix}, \quad (6)$$

where $[A]$ is defined in Eq. (5) and

$$[B^i] = \frac{1}{R}\left([\Lambda](1 + d\lambda^i) + 2R\,\underline{\phi}_c\,\underline{\phi}_c^T - \omega^2[I]\right). \quad (7)$$

Next, we reduce the normal coordinate transfer matrix to a 2x2 transfer matrix. We note that the deflection of the ith component system at the constraint location, $w^i(x_c) \equiv w_c^i$, is the coupling coordinate between subsystems. It can be expressed in terms of the normal coordinate amplitudes as

$$w_c^i = \underline{\phi}_c^T\,\underline{\eta}^i, \quad (8)$$

Combining Eqs. (6) and (8), we obtain the 2x2 displacement transfer matrix* for the ith bay, which relates the constraint deflections at adjacent sites (see the detailed derivation in Appendix A):

$$\begin{bmatrix} w_c^{i+1} \\ w_c^i \end{bmatrix} = [T^i] \begin{bmatrix} w_c^i \\ w_c^{i-1} \end{bmatrix}, \quad \text{with} \quad [T^i] = \begin{bmatrix} \beta^i & -1 \\ 1 & 0 \end{bmatrix}, \quad (9)$$

where the expression of β^i is given in Appendix A.

For a disordered system the $[T^i]$'s are random transfer matrices, their average matrix being that of the ordered structure,

$$[T^o] = \begin{bmatrix} \beta^o & -1 \\ 1 & 0 \end{bmatrix}, \quad (10)$$

where β^o is obtained as β^i with $d\lambda^i = 0$.

The displacement amplitudes are expressed in terms of the right- and left-traveling wave amplitudes by the transformation[12,16]

$$\begin{bmatrix} w_c^i \\ w_c^{i-1} \end{bmatrix} = [X] \begin{bmatrix} L^i \\ R^i \end{bmatrix}, \quad (11)$$

where the columns of $[X]$ are the eigenvectors of the ordered displacement transfer matrix $[T^o]$. The transformation matrix can be written as

$$[X] = \begin{bmatrix} 1 & 1 \\ e^{-jk} & e^{jk} \end{bmatrix}, \quad (12)$$

where k is a (complex) wave number related to the excitation frequency, ω, by the dispersion relation. Substituting Eq. (11) into Eq. (9) leads to the introduction of a wave transfer matrix that relates the wave amplitudes at sites i and $i+1$,

$$\begin{bmatrix} L^{i+1} \\ R^{i+1} \end{bmatrix} = [W^i] \begin{bmatrix} L^i \\ R^i \end{bmatrix}, \quad \text{with} \quad [W^i] = [X]^{-1}[T^i][X]. \quad (13)$$

One can show, for real wave number k (or, equivalently, for frequencies in the passbands),

$$[W^i] = \begin{bmatrix} \frac{1}{t^i} & -\frac{r^i}{t^i} \\ -\frac{(r^i)^*}{(t^i)^*} & \frac{1}{(t^i)^*} \end{bmatrix}, \quad (14)$$

where * denotes a complex conjugate, and t^i and r^i are the complex transmission and reflection coefficients for the ith bay.

For an ordered site, the wave transfer matrix is diagonal consisting of the eigenvalues of $[T^o]$, and there is no reflection. For excitation frequencies such that k is real, there is no attenuation, and such frequencies define a passband. For k not real, there is attenuation, and the frequency belongs to a stopband. For a disordered site, $[X]$ does not diagonalize $[T^i]$, and thus there is reflection ($r^i \neq 0$). This multiple scattering from the random sites leads to the occurrence of localization.

* An exact formulation for the displacement transfer matrix is possible for an assembly of cantilevered Euler-Bernoulli beams. This was used to check the convergence of the component mode analysis. In all cases excellent agreement was observed.

We now consider the transmission of a wave of amplitude a, incident from the left, through an N-site disordered system ($i = 1, \cdots, N$) embedded in an otherwise ordered infinite system. The wave transfer matrix for the disordered segment relates the wave amplitudes entering and leaving it. Specifically, for frequencies in a passband:

$$\begin{bmatrix} L^{N+1} \\ R^{N+1} \end{bmatrix} = [\mathbf{W^N}] \begin{bmatrix} L^1 \\ R^1 \end{bmatrix},$$

$$[\mathbf{W^N}] = \left(\prod_{i=N}^{1} [W^i]\right) = \begin{bmatrix} \frac{1}{\tau^N} & -\frac{\rho^N}{\tau^N} \\ -\frac{(\rho^N)^*}{(\tau^N)^*} & \frac{1}{(\tau^N)^*} \end{bmatrix}, \quad (15)$$

where τ^N and ρ^N are the transmission and reflection coefficients for the disordered segment. Since there is no reflection for the tuned sites, $R^1 = a$ and $L^{N+1} = 0$. It follows that the ratio of the amplitude transmitted through the disordered segment to the incident amplitude is the transmission coefficient, τ^N. Thus, the rate of exponential decay of the transmitted wave amplitude is

$$\gamma_N = -\frac{1}{N} \ln \left| \frac{R^{N+1}}{a} \right| = -\frac{1}{N} \ln |\tau^N|, \quad (16)$$

and its limiting value for an infinite assembly is

$$\gamma = \lim_{N \to \infty} -\frac{1}{N} \ln |\tau^N|, \quad (17)$$

which is determined by the (1,1) term in the overall wave transfer matrix. Equation (17) means that, asymptotically, the transmission coefficient decays exponentially with N at the rate γ. For $\gamma > 0$, the vibrational energy injected into the system is *confined* near the excitation source. For an ordered system γ is the real part of the propagation constant[17]. For a disordered system it is called the localization factor.

3.3 Modal Formulation

The vibration amplitude transmitted to the right end of the assembly due to a left end excitation can be calculated by applying the modal analysis technique first developed by Herbert and Jones[10] and later used by Hodges and Woodhouse[9] and Pierre[14]. This modal formulation was not retained for the analytical evaluation of the localization factors because the wave approach leads to simpler calculations, but it was used in some of the Monte Carlo simulations when the wave approach failed to provide satisfactory results. From Eq. (3), the normal coordinates of the Nth component system can be written as

$$\underline{\eta}^N = [F_{1N}] \frac{F}{\mathcal{M}} \underline{\phi}_f, \quad (18)$$

where $[F_{1N}]$ is the $(1,N)$th MxM submatrix of $([K] - \omega^2[I])^{-1}$, which can be obtained recursively by exploiting tridiagonality[18]. Hence the steady state response amplitude of the Nth component system at the constraint location is

$$\left| \frac{w_c^N}{F/\mathcal{M}} \right| = \left| \underline{\phi}_c^T [F_{1N}] \underline{\phi}_f \right|, \quad (19)$$

which yields, assuming exponential decay of the amplitude,

$$\gamma_N = -\frac{1}{N} \ln \left| \underline{\phi}_c^T [F_{1N}] \underline{\phi}_f \right|. \quad (20)$$

While Eq. (20) does not necessarily imply exponential decay, we are interested in the limiting behavior of γ_N as N approaches infinity. If $\gamma = \lim_{N \to \infty} \gamma_N$, then, asymptotically, the vibration amplitude decays exponentially with N at the rate γ.

4. PASSBANDS AND STOPBANDS OF THE ORDERED SYSTEM

The real part of the propagation constant, γ, is calculated for an infinite ordered assembly over the entire frequency spectrum by the wave formulation.

4.1 Propagation Constant

For the ordered system, the displacement transfer matrix $[T^o]$ is given by Eq. (10), where β^o is a function of ω. The eigenvalues of $[T^o]$ are

$$\lambda_{1,2} = \frac{\beta^o}{2} \pm \sqrt{\left(\frac{\beta^o}{2}\right)^2 - 1}\,, \tag{21}$$

such that $\lambda_1\lambda_2 = 1$. The modal and wave transfer matrices are

$$[X] = \begin{bmatrix} 1 & 1 \\ \frac{1}{\lambda_1} & \frac{1}{\lambda_2} \end{bmatrix} \qquad [W^o] = \begin{bmatrix} \lambda_1 & 0 \\ 0 & \lambda_2 \end{bmatrix}. \tag{22}$$

For the ordered assembly the decay is identical for all sites, hence $\tau^N = 1/\lambda_1^N$. From Eq. (17), the exponential decay constant is simply $\gamma = \ln|\lambda_1|$. Several cases are considered.

- For $\left|\frac{\beta^o(\omega)}{2}\right| < 1$, λ_1 and λ_2 are complex conjugates of modulus 1. Letting $\frac{\beta^o}{2} = \cos k$, for $0 < k < \pi$, we obtain $\lambda_{1,2} = \exp(\pm jk)$, where k is the real wave number. This readily yields $\gamma = 0$. Thus, frequencies such that $\left|\frac{\beta^o(\omega)}{2}\right| < 1$ define the *passbands* of the system. It can be shown that for a given wave number k, $(\beta^o(\omega^2) - 2\cos k)$ has M zeros, defining M frequency bands[16].
- For $\left|\frac{\beta^o(\omega)}{2}\right| > 1$, λ_1 and λ_2 are real. The wave number is complex and γ is positive, leading to attenuation. The corresponding frequencies define the *stopbands*.
- For $\left|\frac{\beta^o(\omega)}{2}\right| = 1$, there is a double eigenvalue $\lambda_1 = \lambda_2 = 1$ or -1. Thus $\gamma = 0$, and the corresponding frequencies define the *passband-stopband edges*. The M zeros of $(\beta^o(\omega^2) - 2)$ define the lower limits of the passbands, $(\omega^2_{p_l})_{p=1,\cdots,M}$, while the zeros of $(\beta^o(\omega^2) + 2)$ give the upper limits, $(\omega^2_{p_u})_{p=1,\cdots,M}$. For an exact representation of the assembly ($M \to \infty$) the number of passbands is infinite.

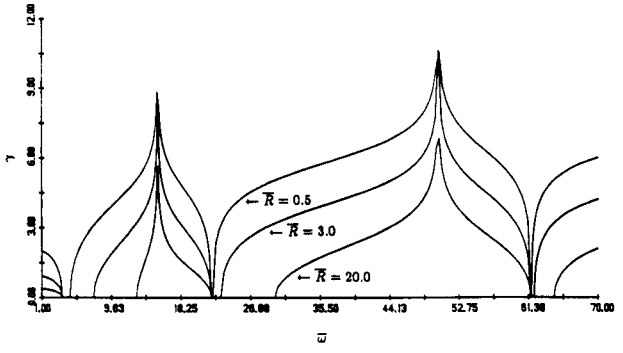

Fig. 3 Exponential decay constant, γ, versus excitation frequency for the first three passbands of an ordered system. The coupling constraint is at the tip ($x_c = 1.0$).

4.2 Results And Remarks

Figure 3 illustrates the alternating bands of attenuation and propagation for an assembly of Euler-Bernoulli beams. The first band is a stopband, where γ decreases to zero as the frequency increases to reach the first passband. In the passbands, γ is identically zero and waves propagate without attenuation. In the second and higher stopbands, we note that γ becomes large and tends to infinity at some particular frequencies (these peaks are probably due to the poles of $\beta^o(\omega^2)$). The effect of spring stiffness is clearly illustrated in Fig. 3: an increase in coupling between the subsystems results in smaller values of the propagation constant and in a widening of the passbands. This is expected because vibration transmission is easier for larger coupling. Also, the width of the passbands diminishes rapidly with increasing passband number, a phenomenon observed for the free vibration frequencies[7]. This is because an increase in the component mode number, p, results in a decrease in the dynamic coupling, R/λ_p (the square of the ratio of the coupling frequency to the pth component frequency). Thus, propagation becomes more difficult as the dynamic coupling decreases, or as p increases.

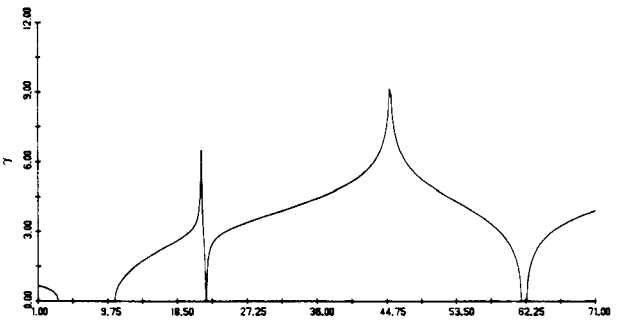

Fig. 4.a.

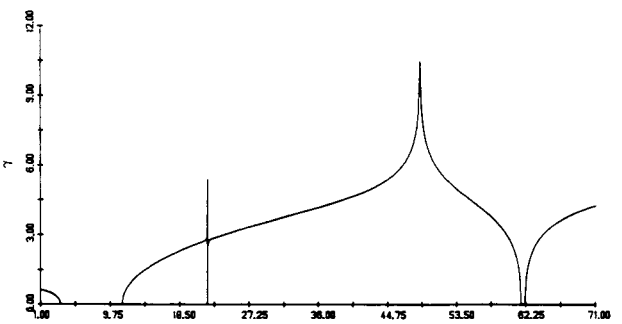

Fig. 4.b.

Fig. 4 Exponential decay constant, γ, versus excitation frequency for the first three passbands of an ordered system with $x_c = 0.75$ (4.a) and $x_c = 0.78$ (4.b). The nondimensional coupling is $\overline{R} = 15.0$.

The effect of constraint location on the propagation constant is displayed in Fig. 4. Here the static coupling is strong and the constraint is at $x_c = 0.75$ and 0.78, near the node of the second mode of the nominal beam ($x = 0.7844$). We note the severe narrowing of the second passband accompanied by the shifting of the stopband peak toward the left edge of the second passband. As the coupling constraint moves closer to the node, the peak of the stopband practically superposes onto the second passband and the corresponding frequency bandwidth becomes negligible. Thus, positioning the coupling constraint very close, or at the node of a component mode practically eliminates the corresponding passband.

The bounding frequencies of the passbands are of importance. The lower limits of the passbands were found to be independent of the coupling $\overline{R}$ and the constraint location x_c, and simply equal to the pth frequency of the nominal subsystem. As a check, the passband-stopband edges were obtained by considering the free vibration natural frequencies of the tuned assembly. For an infinite assembly ($N \to \infty$), these frequencies are known to lie densely in the passbands, with the lowest and highest frequencies in each cluster corresponding to the passband edges[17]. In all cases, the passband edges obtained by the wave formulation were found to be identical to the bounding free vibration frequencies recently obtained by Cha and Pierre[19].

System Size, N	Average γ_N	Variance of γ_N
10	-0.037902	0.009977
50	-0.007798	0.000427
100	-0.003859	0.000155
150	-0.002665	0.000042
200	-0.001557	0.000015
300	-0.001515	0.000012
500	-0.000960	0.000006

TABLE 1: Effects of end conditions on the propagation constant. Values of γ_N obtained by the modal approach, Eq. (20), for *ordered* assemblies of N component systems. The first passband is considered, for $\overline{R} = 3.0$ and $x_c = 1.0$. The first column gives the number of component systems in the assembly, while the second column lists the average of γ_N for eighty frequencies equally spaced in the first passband. The third column gives the estimate of the variance of these eighty values. Recall that for an infinite periodic system, $\gamma = 0$.

Approximations of γ were also obtained numerically by the modal approach, Eq. (20), for finite assemblies. The purpose was to evaluate the effects of boundary conditions on the propagation constant. For all cases considered the force is applied at the tip ($x_f = 1.0$), which ensures that all the modes are excited with equal magnitude. For an N-beam assembly, the modal formulation results in small but nonzero values of γ_N in the passbands, because of the end conditions. Table 1 shows that while for small systems the boundaries affect γ significantly, their effects become negligible as N increases. However, these values must be compared to those of the localization factor for disordered systems.

5. LOCALIZATION FACTORS OF THE DISORDERED SYSTEM

In general localization factors cannot be calculated in closed form and one must resort to numerical Monte Carlo simulations. However, analytical approximations of γ can be obtained in the two limiting cases of strong and weak modal coupling. This is presented in this section with the aid of probabilistic perturbation methods. Since strong attenuation already occurs for the tuned system in the stopbands, the focus lies on disorder effects in the passbands. The mistunings $d\lambda^i$ are assumed to be independent and identically distributed random variables of mean zero and standard deviation σ.

5.1 Small Disorder To Coupling Ratio

Here we assume that the elements of $R\underline{\phi}_c\underline{\phi}_c^T$ are much larger than those of $d\lambda^i[\Lambda]$. Thus:

$$O(\frac{\sigma}{R\,\phi_p^2/\lambda_p}) < 1 \qquad p = 1, \cdots, M\,, \tag{23}$$

where $O(.)$ denotes the order of the argument, and $R\phi_p^2/\lambda_p$ is the "modal" coupling in the pth component mode, or the pth passband. Since the standard deviation of disorder, σ, is small, Eq. (23) implies that the modal coupling is finite or large[7]. A classical perturbation method (CPM) that treats disorder as the perturbation is applied to the wave formulation to derive an analytical expression for the localization factor.

For frequencies inside (or near) the pth passband, it proves convenient to rewrite the (1,1) term of the transfer matrix $[T^i]$ as, from Eq. (A9)

$$\beta^i = \frac{\lambda_p}{R\,\phi_p^2}\left(E_p^i - \underline{F}_p^{i^T}[G_p^i]^{-1}\underline{F}_p^i\right) \qquad (p = 1, \cdots, M) \tag{24}$$

Strictly speaking, the expression (24) holds for all values of p and for a given p it is valid for all frequencies. However, for frequencies in the pth passband, it appeared preferable to use the pth representation of β^i. The derivation of Eq. (24) is justified in Appendix B.

The random displacement matrix for the ith site can be written

$$[T^i] = \begin{bmatrix}\beta^i & -1\\ 1 & 0\end{bmatrix} = \begin{bmatrix}\beta^o & -1\\ 1 & 0\end{bmatrix} + \begin{bmatrix}\delta\beta^i & 0\\ 0 & 0\end{bmatrix} = [T^o] + [\delta T^i]\,, \tag{25}$$

where, to the first order (see Appendix B for the detailed derivation)

$$\begin{cases} \beta^o = \dfrac{\lambda_p}{R\,\phi_p^2}\left(E_p^o - \underline{F}_p^{o^T}[G_p^o]^{-1}\underline{F}_p^o\right) \qquad (p = 1, \cdots, M) \\ \delta\beta^i \simeq \dfrac{\lambda_p\, d\lambda^i}{R\,\phi_p^2}\left(e_p^o - \underline{F}_p^{o^T}[G_p^o]^{-1}\underline{f}_p^o - \underline{f}_p^{o^T}[G_p^o]^{-1}\underline{F}_p^o \right. \\ \qquad\qquad \left. + \underline{F}_p^{o^T}[G_p^o]^{-1}[g_p^o][G_p^o]^{-1}\underline{F}_p^o\right) \\ \qquad = \dfrac{\lambda_p}{R\,\phi_p^2}\,\alpha_p\, d\lambda^i \qquad (p = 1, \cdots, M) \end{cases} \tag{26}$$

where α_p is a function of x_c and ω.

In a passband, the random wave transfer matrix for the ith site is

$$[W^i] = [X]^{-1}\left([T^o] + [\delta T^i]\right)[X] = [W^o] + [\delta W^i]\,, \tag{27}$$

where $[X]$ is the matrix of eigenvectors of $[T^o]$. We obtain

$$\begin{cases} [W^o] = \begin{bmatrix} e^{jk} & 0 \\ 0 & e^{-jk}\end{bmatrix} \\ [\delta W^i] \simeq -j\left(\dfrac{d\lambda^i}{2\sin k}\right)\left(\dfrac{\lambda_p\,\alpha_p}{R\,\phi_p^2}\right)\begin{bmatrix} e^{jk} & e^{jk} \\ -e^{-jk} & -e^{-jk}\end{bmatrix}, \end{cases} \tag{28}$$

where k is such that $\cos k = \frac{\beta^o}{2}$.

The wave transfer matrix for an N-site disordered segment is, to the first order in $\frac{\sigma\lambda_p}{R\phi_p^2}$,

$$[\mathbf{W^N}] = \prod_{i=N}^{1}\left([W^o] + [\delta W^i]\right) \simeq [W^o]^N + \sum_{l=1}^{N}[W^o]^{l-1}[\delta W^{N-l+1}][W^o]^{N-l} + O'\left(\frac{\sigma^2\lambda_p^2}{R^2\phi_p^4}\right), \tag{29}$$

where $O'(\frac{\sigma^2\lambda_p^2}{R^2\phi_p^4})$ consists of terms $d\lambda^l\, d\lambda^m$ for $l \neq m$. We take the modulus of the (1,1) term in Eq. (29) to calculate the localization factor:

$$\gamma = \lim_{N\to\infty}\frac{1}{2N}\ln\left|1 + \frac{\alpha_p^2\,\lambda_p^2}{4R^2\,\phi_p^4\sin^2 k}\left(\sum_{l=1}^{N} d\lambda^l\right)\left(\sum_{m=1}^{N} d\lambda^m\right) + O'\left(\frac{\sigma^2\,\lambda_p^2}{R^2\,\phi_p^4}\right)\right|. \tag{30}$$

Since the mistunings are uncorrelated and identically distributed,

$$\lim_{N\to\infty}\frac{1}{N}\sum_{l,m=1}^{N} d\lambda^l\, d\lambda^m = \sigma^2\,\delta_l^m\,. \tag{31}$$

Hence all terms for $l \neq m$ vanish, which justifies retaining only the first-order terms. Finally, approximating $\ln|1+z|$ by z, we obtain

$$\gamma = \frac{\sigma^2\,\lambda_p^2\,\alpha_p^2}{8R^2\,\phi_p^4\sin^2 k} + O\left(\frac{\sigma^4\,\lambda_p^4}{R^4\,\phi_p^8}\right). \tag{32}$$

Using the dispersion relation $\beta^o(\omega) = 2\cos k$ gives the localization factor in terms of frequency:

$$\gamma^{(c)}(\omega) = \frac{\sigma^2 \lambda_p^2 \alpha_p^2(\omega)}{8R^2 \phi_p^4 (1 - \frac{\beta^{o2}(\omega)}{4})} \qquad (p = 1, \cdots, M), \qquad (33)$$

where $\gamma^{(c)}$ denotes the *classical* perturbation approximation of the localization factor, which holds in the strong modal coupling case. Though Eq. (33) is valid for all values of p and all frequencies, the pth representation of γ is preferred for frequencies in the pth passband, as it exhibits the dependence of the localization factor on modal coupling.

If the pth component mode contributes largely to the motion of the assembly in the pth passband, we can use a *single-mode* approximation for frequencies in the pth passband. Then $\beta^o = (\lambda_p + 2R\phi_p^2 - \omega^2)/(R\phi_p^2)$, $\alpha_p = 1$, and the wave number k is related to frequency by

$$\omega_p^2 = \lambda_p + 4R\,\phi_p^2 \sin^2 \frac{k}{2}, \quad 0 \le k \le \pi, \quad p = 1, \ldots, M, \qquad (34)$$

where λ_p and $(\lambda_p + 4R\,\phi_p^2)$ are the pth passband edges, and ω_p lies in the pth passband. Thus, the one-mode approximation of the localization factor is

$$\gamma^{(c)}(\omega_p) \simeq \frac{\sigma^2}{2(\frac{\omega_p^2}{\lambda_p} - 1)(1 + 4\frac{R\phi_p^2}{\lambda_p} - \frac{\omega_p^2}{\lambda_p})}. \qquad (35)$$

We can make some observations about the localization factor $\gamma^{(c)}$. First, in the pth passband, the classical approximation is only valid for small values of $\frac{\sigma}{R\phi_p^2/\lambda_p}$, the ratio of mistuning to modal coupling. Second, $\gamma^{(c)}$ goes to infinity at the passband-stopband edges. Thus, we expect the classical approximation to deteriorate near the stopbands. Finally, for a given constraint location, x_c, $\gamma^{(c)}$ is primarily* a function of the ratio of mistuning to modal coupling, the same that governs the strong localization of the free modes[7]. Eq. (35) shows that this is exact for a one-mode analysis.

5.2 Large Disorder To Coupling Ratio

Here we assume that the elements of $d\lambda^i[\Lambda]$ are much larger than those of $R\underline{\phi}_c\underline{\phi}_c^T$. Thus, $O(\frac{\sigma}{R\phi_p^2/\lambda_p}) > 1$. Since the disorder is small, this implies that the modal coupling is weak. Note that even for arbitrarily large static coupling, weak modal coupling inevitably occurs at high frequencies, because λ_p increases rapidly with the passband number p. Here we use a modified perturbation method (MPM) which treats coupling as the perturbation, while including disorder in the unperturbed system to avoid degeneracy[2]. This yields

$$[T^i] = [T^{oi}] + [\delta T] \quad , \qquad [T^{oi}] = \begin{bmatrix} \beta^i & 0 \\ 0 & 0 \end{bmatrix} \qquad [\delta T] = \begin{bmatrix} 0 & -1 \\ 1 & 0 \end{bmatrix}, \qquad (36)$$

where, in this weak coupling case, $|\beta^i|$ is much larger than 1. Since the unperturbed matrix is diagonal, no transformation is needed to obtain the wave transfer matrix; thus, $[W^i] \equiv [T^i]$. We note in passing that the modified perturbation scheme is valid in both passbands and stopbands. To the first order in the modal coupling to disorder ratio, the wave transfer matrix for an assembly of size N is

$$[\mathbf{W^N}] = \prod_{i=N}^{1} \left([T^{oi}] + [\delta T]\right) \simeq \prod_{i=N}^{1} [T^{oi}] + \sum_{l=1}^{N} \left(\left(\prod_{i=N}^{l+1} [T^{oi}] \right) [\delta T] \left(\prod_{i=l-1}^{1} [T^{oi}] \right) \right). \qquad (37)$$

A little algebra shows that the first-order terms in Eq. (37) do not contribute to $[\mathbf{W^N}]$. Thus, from Eq. (17),

$$\gamma^{(m)}(\omega) = \lim_{N\to\infty} \frac{1}{N} \sum_{i=1}^{N} \ln\left|\beta^i\right|, \qquad (38)$$

where $\gamma^{(m)}$ is the weak coupling approximation of the localization factor. Considering β as a function of the continuous disorder random variable, ϵ (by definition, $\beta(\epsilon = d\lambda^i) \equiv \beta^i$), Eq. (38) becomes

$$\gamma^{(m)}(\omega) = \frac{1}{2W} \int_{-W}^{W} \ln\left|\beta(\epsilon)\right| d\epsilon, \qquad (39)$$

where the probability density function of disorder is assumed to be uniform of width $2W$ ($\sigma = W/\sqrt{3}$). For a multi-mode system, it is impractical to obtain an analytical expression for $\gamma^{(m)}$ and we evaluate the integral (39) numerically.

However, because the coupling is weak, a single-mode analysis that uses the pth modal representation of the nominal component system is often sufficient to capture the behavior of the assembly in the pth passband. Then,

$$\beta^i \simeq \frac{(1 + d\lambda^i)\lambda_p + 2R\phi_p^2 - \omega_p^2}{R\phi_p^2}, \qquad (40)$$

where ω_p is an excitation frequency in the vicinity of the pth passband. Since β^i is a linear function of the mistuning $d\lambda^i$, β in Eq. (39) is linear in ϵ, which allows for easy integration. Substitution of Eq. (40) into Eq. (39) gives the one-mode approximation of the modified perturbation result, valid only in the vicinity of the pth passband:

$$\gamma^{(m)}(\omega_p) \simeq -1 - \ln\left|\frac{R\phi_p^2}{\lambda_p}\right| + \frac{1 + W + \frac{2R\phi_p^2}{\lambda_p} - \frac{\omega_p^2}{\lambda_p}}{2W} \ln\left|1 + W + \frac{2R\phi_p^2}{\lambda_p} - \frac{\omega_p^2}{\lambda_p}\right| - \frac{1 - W + \frac{2R\phi_p^2}{\lambda_p} - \frac{\omega_p^2}{\lambda_p}}{2W} \ln\left|1 - W + \frac{2R\phi_p^2}{\lambda_p} - \frac{\omega_p^2}{\lambda_p}\right|. \qquad (41)$$

6. PERTURBATION AND SIMULATION RESULTS

These analytic perturbation results are verified by Monte Carlo simulations for assemblies of clamped Euler-Bernoulli beams with random flexural rigidities. Simulations can be performed either by the wave or the modal formulation, by averaging the rate of decay γ_N in Eqs. (16) and (20) over many realizations of disorder. A key difference is that the modal scheme accounts for boundary conditions, while the wave method does not. Because no engineering structure is infinite, the modal approach is probably better suited in most engineering applications. The modal simulation requires the inversion of $r \times N_m$ matrices of size M for each frequency, where r is the number of realizations in the ensemble and N_m the (modal) number of component beams. Similarly, for the wave simulation, $r \times N_w$ matrices of size $(M-1)$ must be inverted, where N_w is the (wave) number of sites. However, to offset the effect of boundary conditions, the modal scheme requires a much larger number of component beams than the wave simulation. This is particularly true when the localization effect is very weak, since the decay factor due to disorder must be orders of magnitude larger than that arising inevitably from boundary conditions. On the other hand, by the wave simulation, the dependence of γ on N_w was found to be small for weak localization effects, therefore few subsystems were needed. Thus, in general, $N_m \gg N_w$, and wave simulations are considerably less expensive than modal ones. However, for strong localization effects, we observed that a modal simulation (albeit more expensive) tracks the analytical result much better than a wave simulation, especially in the stopbands. Though why this is the case is not clear, one should not hastily discard the modal

* The coefficient α_p was found to be approximately constant as p varies.

approach in favor of the wave formulation. In short, both methods complement one another.

To keep the computer cost reasonable, 500 realizations each with 50 random sites are considered for the modal approach. This ensures that the standard error* for the localization factor is consistently several orders of magnitude smaller than the mean. For the less expensive wave simulation, configurations are chosen according to the system parameters and are specified for each case considered.

Figure 5 displays the localization factor versus frequency for $\overline{R} = 3.0, x_c = 1.0$, and $\sigma = 2.0\%$. The modal coupling, $\overline{R}\phi_p^2/\overline{\lambda}_p$, decreases rapidly as the passband number increases, because for a cantilevered beam $\overline{\lambda}_p$ increases asymptotically as $\overline{\lambda}_p \simeq [\frac{(2p-1)\pi}{2}]^4$. The ratios of disorder to modal coupling for passbands one to four, $(\sigma/(\overline{R}\phi_p^2/\overline{\lambda}_p))_{p=1,\ldots,4}$, are 0.021, 0.809, 6.344 and 24.362, respectively. Therefore, we used the perturbation method for strong coupling case (Eq. (33)) in the first two passbands, while we chose the weak coupling scheme (Eq. (39)) for the last two. For both classical and modified perturbation results we used the full *multi-mode* representation of the subsystems. To validate the theoretical results, we performed wave and modal Monte Carlo simulations in the first two and last two passbands, respectively. We used the modal simulation in the vicinity of the third and fourth bands because we found that the wave simulation results deteriorate rapidly in the stopbands. We chose a configuration of 750 realizations of 10 random sites for the wave simulation, although we observed that taking only two random sites gives accurate results as well.

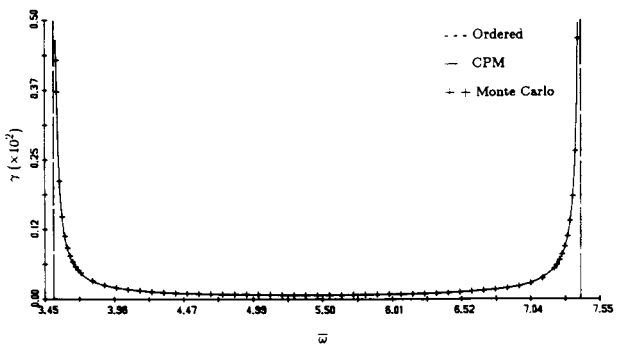

Fig. 5.a. First passband.

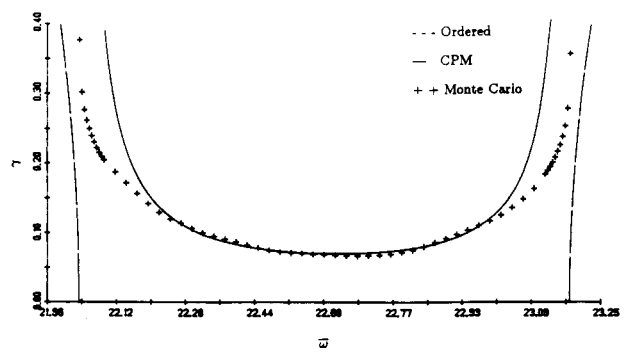

Fig. 5.b. Second passband.

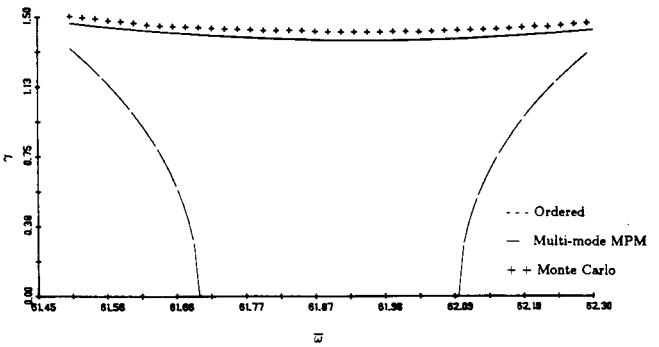

Fig. 5.c. Third passband.

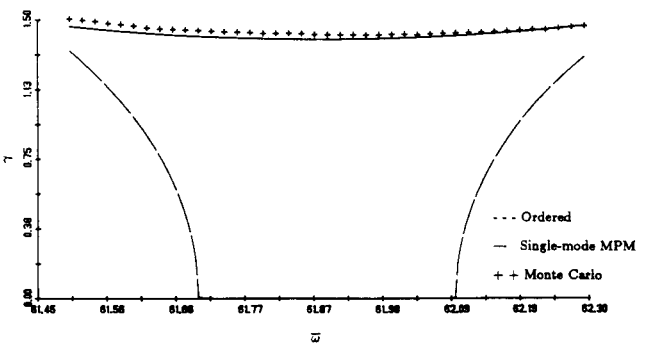

Fig. 5.d. Third passband.

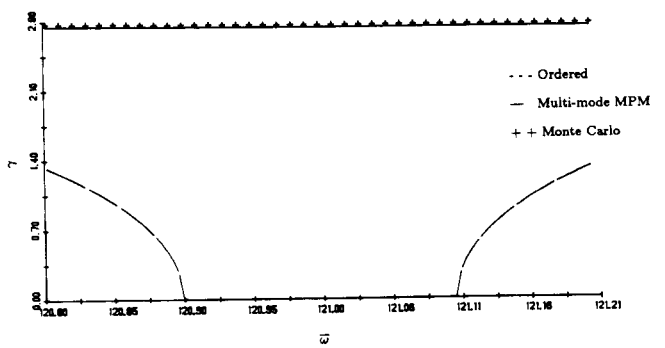

Fig. 5.e. Fourth passband.

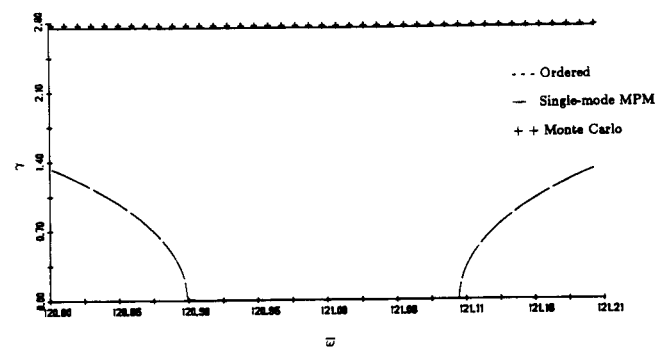

Fig. 5.f. Fourth passband.

Fig. 5 Localization factor in the first four frequency passbands, for $x_c = 1.0$, $\overline{R} = 3.0$ and $\sigma = 2.0\%$.

* The standard error is defined as the estimate of the standard deviation of the localization factor divided by the square root of the number of realizations in the simulation.

The strong frequency dependence of γ in the first two passbands is readily observed in Fig. 5: the localization effect is maximum near the stopbands, an expected trend, and minimum near the midband. A consequence is that normal modes in the same passband can have very different degrees of localization.† The agreement between the theoretical and simulation results is excellent in the first passband, where localization is very weak. The localization factor around midband increases approximately 1,000-fold from the first to the second passband. The agreement between simulation and theory is good over most of the second passband, except near the stopbands where the perturbation results overpredict the simulations; this is expected since $\gamma^{(c)} \to \infty$ at the passband edges. The agreement between perturbation and simulation becomes worse in the second passband because the CPM approximation deteriorates as the modal coupling decreases. This deterioration takes place first for frequencies leading to large γ, that is, near the passband edges.

Figure 5 shows that the localization effect becomes very strong in the third and fourth passbands. Unlike the weak localization displayed in the first and (to a lesser degree) second passbands, where γ in the stopbands is orders of magnitude larger than in the passbands, for the strong localization case the localization factors in the passbands and the stopbands have comparable magnitude. Also, contrary to the first two passbands, γ varies little with frequency in the third and fourth passbands. Thus, we expect all normal modes to be strongly localized in these passbands. We also note that the agreement between simulation and modified perturbation results is very good in the third passband. It becomes excellent in the fourth band because the modal coupling is smaller. Therefore, a key conclusion from Fig. 5 is that the degree of localization increases rapidly with the component mode number.

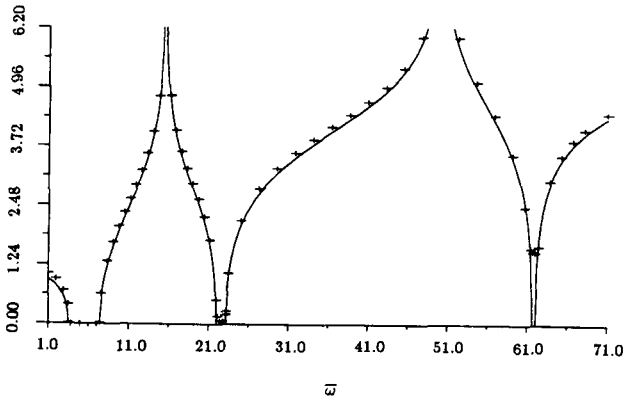

Fig. 6 Localization factor versus frequency, for $x_c = 1.0$, $\overline{R} = 3.0$ and $\sigma = 2.0\%$, by Monte Carlo simulations (+). The decay constant for the tuned system (—) is also shown.

Finally, the single-mode approximation of the MPM result (Eq. (41)) is also shown in Fig. 5. The agreement with simulation is nearly as good as for the multi-mode result, indicating that the much simpler one-mode result is a valid approximation.

Figure 6 illustrates the variation of γ over the first three stopbands and passbands for the system parameters as in Fig. 5. It is clear that for weak modal coupling the third passband is nearly lost for the disordered system and attenuation is very strong. This would even be more pronounced in the fourth passband. Also note that disorder has very little effect on the attenuation in the stopbands.

† Accepting the conjecture by Ishii[13] that the amplitude patterns of forced vibrations and free modes are governed by the same exponential envelope at a given frequency.

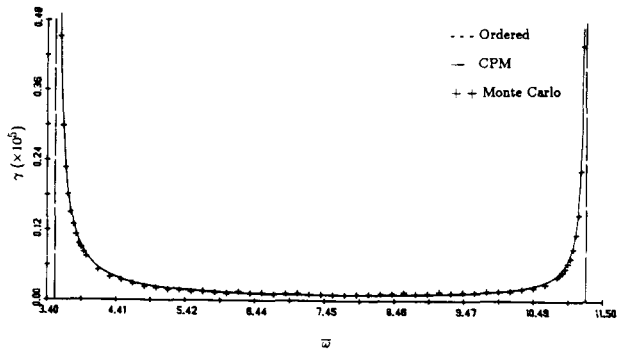

Fig. 7.a. First passband.

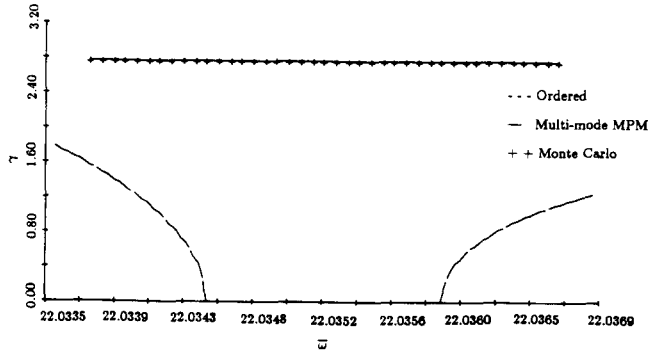

Fig. 7.b. Second passband.

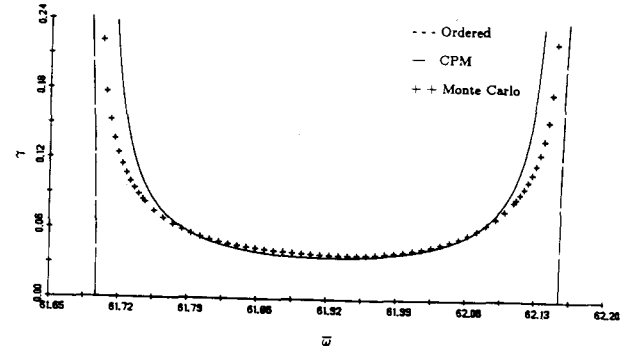

Fig. 7.c. Third passband.

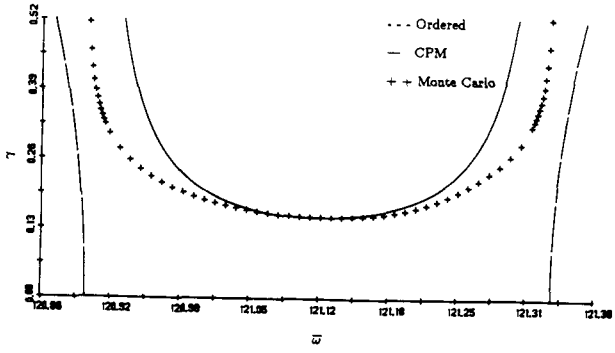

Fig. 7.d. Fourth passband.

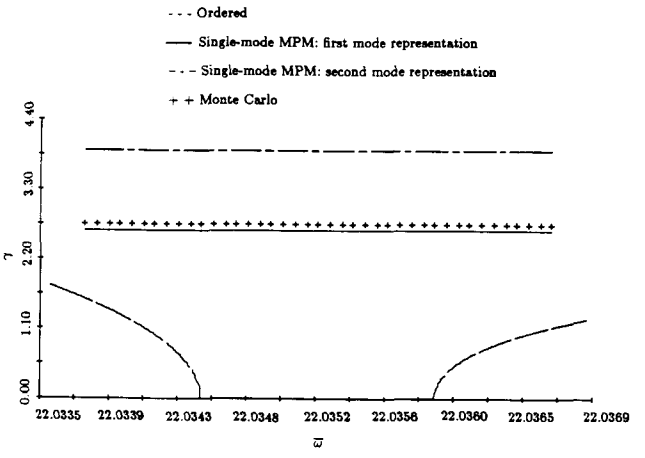

Fig. 7.e. Second passband.

Fig. 7 Localization factor in the first four frequency passbands, for $x_c = 0.78$, $\overline{R} = 15.0$ and $\sigma = 0.2\%$.

Figure 7 illustrates the effect of constraint location on the localization factor. The coupling spring is located at $x_c = 0.78$, very close to the node of the second mode of the nominal beam ($x = 0.7844$); thus, $\phi_2(x_c) \simeq 0$. The static coupling is large ($\overline{R} = 15.0$) and the disorder very small ($\sigma = 0.2\%$). Thus, if the constraint location were at the tip, we would expect γ to be very small in the lower passbands, corresponding to weak localization. From Fig. 7, the localization factor is indeed small for passbands 1, 3 and 4, and increasing from one passband to the next. The agreement between the wave simulation and the classical perturbation method is excellent in the first passband and good at the middle of the third and fourth passbands, though it deteriorates near the edges. Since the coupling constraint is near the node of the second mode, the corresponding modal coupling is very small ($\overline{R}\phi_2^2/\overline{\lambda}_2 \simeq 0.000025$); thus the modified perturbation method is used in the second passband. The agreement between the multi-mode modified perturbation result (numerical evaluation of the integral (39)) and the modal simulation is excellent. We observe that the localization effect in the second passband is severe, due to the location of the constraint. Thus, in this case, there is strong localization in the second passband but weak localization in the neighboring passbands.

We found that the single-mode modified perturbation scheme ($p = 2$ in Eq. (41)) grossly overestimates the localization factor in the second passband (this is shown in Fig. 7.e), even though it gives very good results in cases of small coupling in Fig. 5. We can tentatively explain this by noting that the pth passband is nearly lost when the constraint location is near a node of the pth component mode; thus, the system practically does not vibrate in the pth mode, and the frequency range where the single-mode MPM for the $(p-1)$th passband applies is extended to encompass the pth passband. Indeed, we applied the MPM using the *first* modal representation ($p = 1$ in Eq. (41)) for frequencies in the neighborhood of the *second* passband. Figure 7.e shows that the maximum difference between the γ's obtained with MPM and simulation is less than 4%. This confirms our conjecture.

7. LOCALIZATION FACTORS AT MIDBAND

The dependence of the localization factor on the ratio of disorder strength to modal coupling and the passband number is investigated by considering the localization factor at the midband excitation frequencies, $(\omega_{p_m})_{p=1,\cdots,M}$. These frequencies are obtained from the dispersion relation for $k = \frac{\pi}{2}$, or $\beta^o = 0$. In the strong coupling case, Eq. (33) gives the classical approximation of the localization factor at midband,

$$\gamma_{p_m}^{(c)} = \frac{\sigma^2 \alpha_{p_m}^2}{8R^2 \phi_p^4/\lambda_p^2} . \tag{42}$$

The single-mode approximation of the localization factor at midband, obtained from Eq. (35), is given by Eq. (42) for $\alpha_{p_m} = 1$. For weak coupling, the single-mode approximate modified perturbation scheme is used; Eq. (34) gives $\omega_{p_m}^2 \simeq \lambda_p(1 + 2\frac{R\phi_p^2}{\lambda_p})$, and Eq. (41) reduces to

$$\gamma_{p_m}^{(m)} \simeq \ln\left|\frac{\sigma}{R\,\phi_p^2/\lambda_p}\right| + \ln\sqrt{3} - 1 . \tag{43}$$

For given constraint location and passband number, α_{p_m} is an explicit function of ω_{p_m}. Since for a given x_c, ω_{p_m} is a function of R, α_{p_m} depends on R implicitly. Upon numerical examination, we found that α_{p_m} remains relatively constant when R varies, especially in the higher passbands, where α_{p_m} is almost perfectly constant equal to one. In the lower passbands, where the CPM is valid, we found that α_{p_m} is a slowly increasing function of R. Thus, from Eq. (42), the localization factor does not vary exactly parabolically with $\sigma/(R\phi_p^2/\lambda_p)$ in the weak localization case, but increases at a slightly slower rate. Eq. (43) exhibits the logarithmic variation with $\sigma/(R\phi_p^2/\lambda_p)$ in the strong localization, or large γ, case. Thus, as the ratio $\sigma/(R\phi_p^2/\lambda_p)$ increases from zero, the localization factor first increases nearly *parabolically*; once it reaches a large value (of the order of 0.5), its increase is more moderate, according to a *logarithmic* law.

Figure 8 shows the variation of γ in terms of the disorder strength, σ, for midband excitation with $\overline{R} = 3.0$ and $x_c = 1.0$. Monte Carlo simulation and multi-mode classical and modified perturbation results are shown for the first four passbands. In the

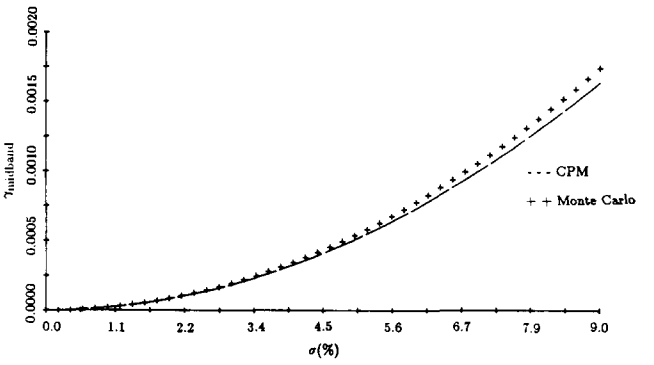

Fig. 8.a. First passband.

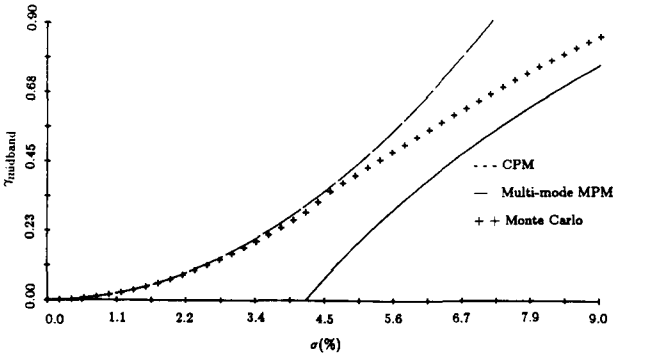

Fig. 8.b. Second passband

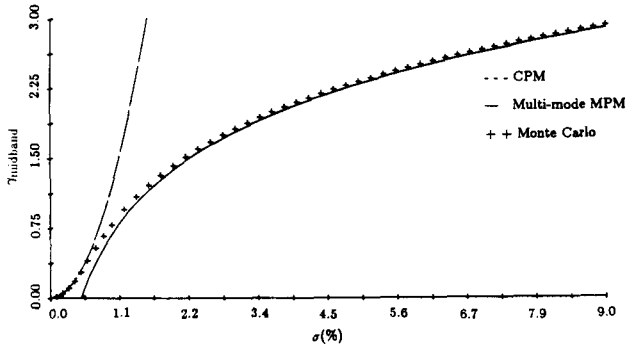

Fig. 8.c. Third passband.

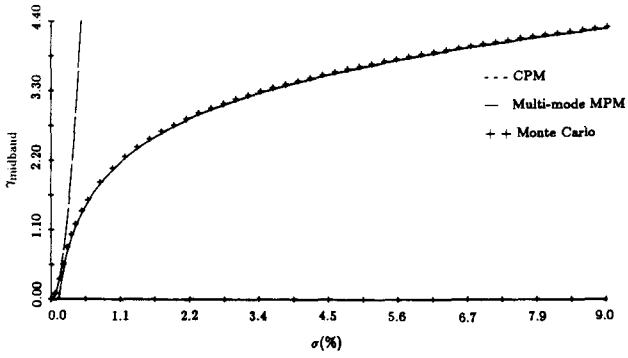

Fig. 8.d. Fourth passband.

Fig. 8 Localization factor versus disorder at midband excitation frequency for the first four passbands, for $\overline{R} = 3.0$ and $x_c = 1.0$.

first passband, where weak localization occurs, the CPM tracks the numerical solution very well until $\sigma = 9\%$. In the second passband, the simulation and CPM results are in excellent agreement as σ increases from zero to approximately 4.5%. As σ keeps increasing, the simulation diverges from the classical perturbation solution, and approaches the modified perturbation result. The Monte Carlo and the modified perturbation results are in excellent agreement in the third and fourth passband for $\sigma > 1.0\%$ and $\sigma > 0.3\%$, respectively, corresponding to strong localization. Only for very small disorder is the CPM a good approximation in these weak coupling cases. Figure 8 displays clearly the transition from parabolic to logarithmic variation (that is, from weak to strong localization) for the localization factor. Similar results can be expected if γ is plotted versus $1/\overline{R}$ instead of σ.

The dependence of γ on disorder strength is also investigated when the constraint is located near a component mode's node (here $x_c = 0.78$, near the second mode's node). Figure 9 shows the variation of γ in terms of σ, for midband excitation frequency and $\overline{R} = 15.0$. Only the second passband is considered, since in other passbands the variation of the localization factor is similar to that in Fig. 8. Figure 9 shows that for very small disorder the CPM approximates γ well, and that as disorder increases the MPM tracks the simulation result remarkably well. Interestingly, the localization factor reaches a saturation value as disorder increases to approximately 0.1%, and remains relatively constant thereafter. Thus, when the coupling constraint is near a node, disorder seems to have an effect only up to a certain point, beyond which an increase in disorder strength does not result in an increase in the localization factor. We found that this saturation value of $\gamma = 2.75$ is approximately equal to the decay factor in the stopbands adjacent to the second passband (this can be seen in Fig. 4b). As discussed in section 6, we were also able to obtain this saturation value of the localization factor by applying the single-mode approximate MPM for $p = 1$.

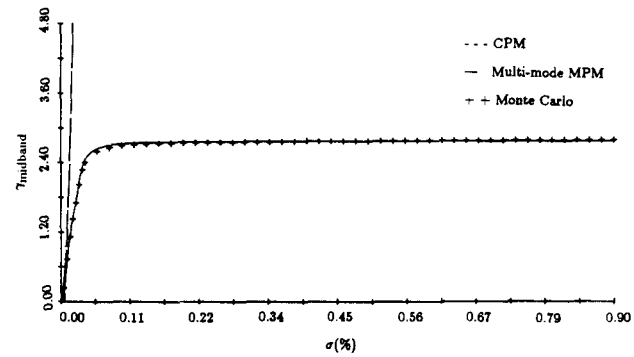

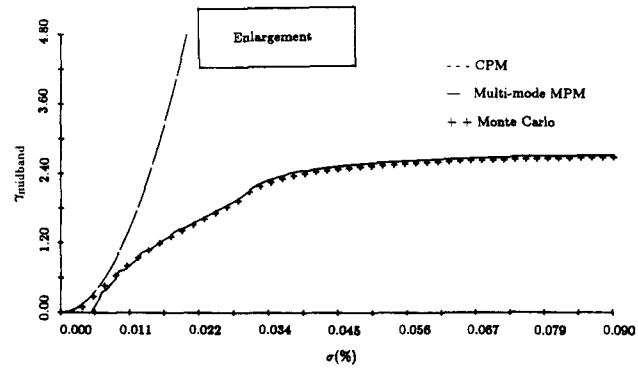

Fig. 9 Localization factor versus disorder at midband excitation frequency for the second passband, for $\overline{R} = 15.0$ and $x_c = 0.78$.

Finally, we consider the dependence of the localization factor on the passband number, p. For a cantilevered beam, the free vibration eigenvalues increase asymptotically as $\overline{\lambda}_p \simeq [\frac{(2p-1)\pi}{2}]^4$. Restricting the analysis to an infinite assembly of cantilevered beams, Eq. (42) becomes

$$\gamma_{p_m}^{(c)} \simeq \frac{\sigma^2 \alpha_{p_m}^2 (2p-1)^8 \pi^8}{2048 \overline{R}^2 \phi_p^4}, \tag{44}$$

while Eq. (43) yields

$$\gamma_{p_m}^{(m)} \simeq 4 \ln|2p-1| + \ln\left|\frac{\sigma \pi^4}{16 \overline{R} \phi_p^2}\right| + \ln\sqrt{3} - 1. \tag{45}$$

For simplicity, we assume that ϕ_p^2 is independent of p.* For the case of weak localization, where the classical perturbation method applies, the localization factor varies approximately as p^8 (exactly so for a one-mode analysis), but only as $(\frac{\sigma}{\overline{R}})^2$. Thus the degree of localization is much more sensitive to the passband number than to either the disorder or the static coupling strength. This implies that the transition from weak to strong localization occurs very rapidly with increasing passband number, which has been observed in Fig. 5 from passband two to passband three. Once the strong localization regime is reached, the degree of localization increases logarithmically with passband number, the same dependence it has on the disorder and coupling strength. This indicates that assemblies of beam-like component systems, such as bladed-disk assemblies, are highly sensitive to very small irregularities, especially at high frequencies where severe localization occurs.

* This is indeed the case for coupling at the tip.

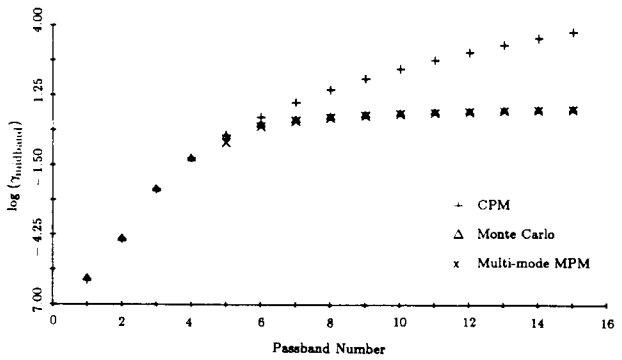

Fig. 10 Midband localization factor versus the passband number, for $\overline{R} = 20.0, \sigma = 0.004$, and $x_c = 1.0$.

This dependence of the localization factor on the passband number is illustrated in Fig. 10. Monte Carlo simulation and classical and modified perturbation results are shown. Note the rapid transition from weak to strong localization and the very good agreement between the simulation and analytical results for all passbands.

8. SIGNIFICANCE OF LOCALIZATION EFFECTS

To illustrate the effects of irregularities on the dynamics of engineering structures, consider the case $\overline{R} = 3.0$, $x_c = 1.0$, and $\sigma = 2\%$. The simulated localization factors at the lower four midband frequencies are 0.00008557, 0.06806, 1.4231, and 2.7624, respectively. Since the vibration amplitude is governed, on the average, by $e^{-\gamma N}$, 8100 sites are needed for the amplitude to decay by a factor of two in the first passband, but only 10 sites are required in the second passband. In terms of energy, only 0.0196% is transmitted to the third site in the third passband, and less than 0.0016% is transmitted to the second site in the fourth passband. Recall that for a perfectly periodic system γ is zero at midband frequencies and 100% of the vibrational energy is transmitted. This spectacular localization is caused by a disorder of strength 2% only, which is difficult to avoid in engineering structures. Also, this phenomenon occurs in a damping-free environment and is solely caused by disorder.

Our study has shown that strong modal coupling and small disorder lead to *weak* localization, such that the amplitude decay per site is very small. In the above example, several thousands subsystems are needed for localization effects to be significant in the first passband. Few, if any, engineering structures consist of so many components. Furthermore, the effects of end conditions and damping may conceal that of disorder completely when the localization factor is so small. Thus, weak localization, though academically interesting, appears to be of little importance in structural dynamics. It is, however, relevant to physicists concerned with very large lattices.

On the other hand, disordered assemblies with weak modal coupling exhibit the phenomenon of *strong* localization: energy is confined near the excitation source and the vibration is transmitted to only a few component systems. We showed that even for very strong static coupling and very weak disorder, strong localization is unavoidable at high frequencies. The placement of the coupling constraint near a node may also cause strong localization to occur. Structural dynamicists should be fully aware of these drastic effects of small disorder.

9. CONCLUSIONS

The effects of periodicity-destroying irregularities on vibration transmission in assemblies of mono-coupled, multi-mode component systems were investigated. Analytical results were derived by probabilistic perturbation methods and confirmed by Monte Carlo simulations.

While for an ordered assembly there are alternate frequency bands of propagation and attenuation, small irregularities result in an exponential amplitude decay for all frequencies. The degree of localization depends primarily on the ratio of disorder to modal coupling: this dependence is nearly parabolic for small values of this ratio, and logarithmic for large values. Localization is very strong for weak internal coupling, and the transition from weak to strong confinement occurs very rapidly with increasing passband number p (for small values, γ varies as p^8). Therefore, severe spatial attenuation of the vibration amplitude is unavoidable at high frequencies, regardless of how large the internal coupling is and how small the disorder is. This has important consequences for the dynamics of mistuned assemblies of beam-like subsystems such as bladed-disk assemblies.

REFERENCES

[1] Hodges, C. H., 1982, "Confinement of Vibration by Structural Irregularity," *Journal of Sound and Vibration*, Vol. 82, No. 3, pp. 411–424.

[2] Pierre, C., and Dowell, E. H., 1987, "Localization of Vibrations by Structural Irregularity," *Journal of Sound and Vibration*, Vol. 114, No. 3, pp. 549–564.

[3] Valero, N. A., and Bendiksen, O. O., 1986, "Vibration Characteristics of Mistuned Shrouded Blade Assemblies," *ASME Journal of Engineering for Gas Turbines and Power*, Vol. 108, No. 2, pp. 293–299.

[4] Bendiksen, O. O., 1987, "Mode Localization Phenomena in Large Space Structures," *AIAA Journal*, Vol. 25, No. 9, pp. 1241–1248.

[5] Cornwell, P. J., and Bendiksen, O. O., 1989, "Localization of Vibration in Large Space Reflectors," *AIAA Journal*, Vol. 27, No. 2, pp. 219-226.

[6] Wei, S. T., and Pierre, C., 1988, "Localization Phenomena in Mistuned Assemblies with Cyclic Symmetry. Part I: Free Vibrations," *ASME Journal of Vibration, Acoustics, Stress, and Reliability in Design*, Vol. 110, No. 4, pp. 429–438.

[7] Pierre, C., and Cha, P. D., 1989, "Strong Mode Localization in Nearly Periodic Disordered Structures," *AIAA Journal*, Vol. 27, No. 2, pp. 227–241.

[8] Cornwell, P. J., and Bendiksen, O. O., 1989, "A Numerical Study of Vibration Localization in Disordered Cyclic Structures," AIAA paper 89-1181-CP, *Proceedings of the 30th Structures, Structural Dynamics and Materials Conference*, Mobile, Alabama.

[9] Hodges, C. H., and Woodhouse, J., 1983, "Vibration Isolation from Irregularity in a Nearly Periodic Structure: Theory and Measurements," *Journal of Acoustical Society of America*, Vol. 74, No. 3, pp. 894–905.

[10] Herbert, D. C., and Jones, R., 1971, "Localized States in Disordered Systems," *Journal of Physics C: Solid State Physics*, Vol. 4, pp. 1145–1161.

[11] Kissel, G. J., 1987, "Localization in Disordered Periodic Structures," AIAA paper 87-0819, *Proceedings of the 28th Structures, Structural Dynamics and Materials Conference*, Monterey, California.

[12] Kissel, G. J., 1988, "Localization in Disordered Periodic Structures," Ph.D. Dissertation, Massachusetts Institute of Technology.

[13] Ishii, K., 1973, "Localization of Eigenstates and Transport Phenomena in the One-Dimensional Disordered System," *Supplement of the Progress of Theoretical Physics*, Vol. 53, pp. 77–138.

[14] Pierre, C., 1989, "Weak and Strong Vibration Localization in Disordered Structures: A Statistical Investigation," *Journal of Sound and Vibration*, Vol. 138, No. 2, April 1990, in press.

[15] Dowell, E. H., 1972, "Free Vibrations of an Arbitrary Structure in Terms of Component Modes," *ASME Journal of Applied Mechanics*, Vol. 39, No. 3, pp. 727–732.

[16] Brillouin, L., 1953, *Wave Propagation in Periodic Structures*, Second Edition, Dover Publications, New York.

[17] Mead, D. J., 1975, "Wave Propagation and Natural Modes in Periodic Systems: I. Mono-Coupled Systems," *Journal of Sound and Vibration*, Vol. 40, No. 1, pp. 1–18.

[18] Przemieniecki, J. S., 1985, *Theory of Matrix Structural Analysis*, Dover Publications, New York.

[19] Cha, P. D., and Pierre, C., 1989, "Eigensolution of Periodic Assemblies of Multi-Mode Component Systems," *Journal of Sound and Vibration*, Vol. 129, No. 1, pp. 168–174.

APPENDIX A: TRANSFER MATRIX DERIVATION

We consider Eq. (6). Since $[A] = \underline{\phi}_c \underline{\phi}_c^T$ is singular, we can express it as $[A] = [L][D][L]^T$, where $[L]$ is nonsingular and $[D]$ diagonal with one nonzero element:

$$[L] = \begin{bmatrix} \phi_1 & 0 & 0 & \dots & 0 \\ \phi_2 & 1 & 0 & \dots & 0 \\ \phi_3 & 0 & 1 & \dots & 0 \\ \vdots & \vdots & \vdots & \ddots & \vdots \\ \phi_M & 0 & 0 & \dots & 1 \end{bmatrix} \qquad [D] = \begin{bmatrix} 1 & 0 & 0 & \dots & 0 \\ 0 & 0 & 0 & \dots & 0 \\ 0 & 0 & 0 & \dots & 0 \\ \vdots & \vdots & \vdots & \ddots & \vdots \\ 0 & 0 & 0 & \dots & 0 \end{bmatrix} . \tag{A1}$$

By moving the column of modal deflections in L to the pth position and having the nonzero element of $[D]$ be the pth diagonal element, it is always possible to have the determinant of $[L]$ be ϕ_p, *i.e.*, the modal deflection for the passband of interest. This enables us to write the transfer matrix in terms of the pth modal representation of the nominal component system, (λ_p, ϕ_p).

Substituting Eq. (A1) into Eq. (6) and pre-multiplying the resulting expression by a 2x2 block diagonal matrix with $[L]^{-1}$ as diagonal blocks gives:

$$\begin{bmatrix} [D][L]^T & [0] \\ [0] & [D][L]^T \end{bmatrix} \begin{bmatrix} \underline{\eta}^{i+1} \\ \underline{\eta}^i \end{bmatrix} = \begin{bmatrix} [L]^{-1} & [0] \\ [0] & [L]^{-1} \end{bmatrix} \begin{bmatrix} [B^i] & -[A] \\ [A] & [0] \end{bmatrix} \begin{bmatrix} \underline{\eta}^i \\ \underline{\eta}^{i-1} \end{bmatrix} . \tag{A2}$$

Using Eq. (2), it is simplified as

$$\begin{bmatrix} \underline{a}^{i+1} \\ \underline{a}^i \end{bmatrix} = \begin{bmatrix} [L]^{-1}[B^i] & -[Q] \\ [Q] & [0] \end{bmatrix} \begin{bmatrix} \underline{\eta}^i \\ \underline{\eta}^{i-1} \end{bmatrix} , \tag{A3}$$

where

$$\underline{a}^i = \begin{bmatrix} w^i(x_c) \\ 0 \\ \vdots \\ 0 \end{bmatrix} , \qquad [Q] = \begin{bmatrix} \phi_1 & \phi_2 & \dots & \phi_M \\ 0 & 0 & \dots & 0 \\ \vdots & \vdots & \ddots & \vdots \\ 0 & 0 & \dots & 0 \end{bmatrix} . \tag{A4}$$

The first equation in Eq. (A3) leads to

$$\begin{bmatrix} w_c^{i+1} \\ 0 \\ \vdots \\ 0 \end{bmatrix} = [L]^{-1}[B^i]\underline{\eta}^i - \begin{bmatrix} w_c^{i-1} \\ 0 \\ \vdots \\ 0 \end{bmatrix} . \tag{A5}$$

Multiplying the first expression on the right hand side of Eq. (A5) by $[L]^{-T}[L]^T$,

$$\begin{bmatrix} w_c^{i+1} \\ 0 \\ \vdots \\ 0 \end{bmatrix} = [L]^{-1}[B^i][L]^{-T} \begin{bmatrix} w_c^i \\ \eta_2^i \\ \vdots \\ \eta_M^i \end{bmatrix} - \begin{bmatrix} w_c^{i-1} \\ 0 \\ \vdots \\ 0 \end{bmatrix} . \tag{A6}$$

Partitioning the matrix product $[L]^{-1}[B^i][L]^{-T}$ yields

$$\begin{bmatrix} w_c^{i+1} \\ \underline{0} \end{bmatrix} = \begin{bmatrix} E^i & \underline{F}^{i^T} \\ \underline{F}^i & [G^i] \end{bmatrix} \begin{bmatrix} w_c^i \\ \underline{\eta}^i \end{bmatrix} - \begin{bmatrix} w_c^{i-1} \\ \underline{0} \end{bmatrix} . \tag{A7}$$

where the dimensions of $E^i, \underline{F}^i$ and $[G^i]$ are 1x1, $(M-1)$x1, and $(M-1)$x$(M-1)$, respectively. Substituting the second equation in (A7) into the first one gives

$$w_c^{i+1} = \left(E^i - \underline{F}^{i^T}[G^i]^{-1}\underline{F}^i\right) w_c^i - w_c^{i-1} , \tag{A8}$$

where $[G^i]$ is nonsingular since $[B^i]$ is positive definite. The displacement transfer matrix which relates the constraint deflections at adjacent sites is therefore

$$\begin{bmatrix} w_c^{i+1} \\ w_c^i \end{bmatrix} = \begin{bmatrix} \beta^i & -1 \\ 1 & 0 \end{bmatrix} \begin{bmatrix} w_c^i \\ w_c^{i-1} \end{bmatrix} , \qquad \beta^i = E^i - \underline{F}^{i^T}[G^i]^{-1}\underline{F}_i . \tag{A9}$$

Once w_c^i is obtained, we may utilize Eqs. (A7) and (A6) to compute $\underline{\eta}^i$, which enables us to calculate the wave modes.

APPENDIX B: TRANSFER MATRIX PERTURBATION EXPANSION

For frequencies in the neighborhood of the pth passband, we factor λ_p in $[B^i]$ to obtain a dimensionless frequency squared, $\frac{\omega^2}{\lambda_p}$:

$$[B^i] = \frac{\lambda_p}{R}[B_p^i] \qquad [B_p^i] = [\overline{\Lambda}](1 + d\lambda^i) + 2\frac{R}{\lambda_p}\underline{\phi}_c\underline{\phi}_c^T - \frac{\omega^2}{\lambda_p}[I] . \tag{B1}$$

where $[\overline{\Lambda}]$ is diagonal of elements $(\lambda_q/\lambda_p)_{q=1,\dots,M}$. We also define $[\overline{L}] = [L]/\phi_p$, such that its pth diagonal element is 1. Thus,

$$[L]^{-1}[B^i][L]^{-T} = \frac{\lambda_p}{R\phi_p^2}[\overline{L}]^{-1}[B_p^i][\overline{L}]^{-T} \tag{B2}$$

which is valid for all values of p, but is intended for use for frequencies in the pth passband. In the case of small disorder to coupling ratio, we write $[B_p^i] = [B_p^o] + [b_p^i]$, where

$$\begin{cases} [B_p^o] = \left([\overline{\Lambda}] + 2\frac{R}{\lambda_p}\underline{\phi}_c\underline{\phi}_c^T - \frac{\omega^2}{\lambda_p}[I]\right) \\ [b_p^i] = [\overline{\Lambda}]d\lambda^i \end{cases} \tag{B3}$$

Thus,

$$\begin{bmatrix} E^i & \underline{F}^{i^T} \\ \underline{F}^i & [G^i] \end{bmatrix} = \frac{\lambda_p}{R\phi_p^2}\begin{bmatrix} E_p^o & \underline{F}_p^{o^T} \\ \underline{F}_p^o & [G_p^o] \end{bmatrix} + \frac{\lambda_p}{R\phi_p^2}\begin{bmatrix} e_p^i & \underline{f}_p^{i^T} \\ \underline{f}_p^i & [g_p^i] \end{bmatrix} , \tag{B4}$$

Substitution of Eq. (B4) into Eq. (A9) gives

$$\beta^i = \frac{\lambda_p}{R\phi_p^2}\left[(E_p^o + e_p^i) - \left(\underline{F}_p^o + \underline{f}_p^i\right)^T \left([G_p^o] + [g_p^i]\right)^{-1} \left(\underline{F}_p^o + \underline{f}_p^i\right)\right] , \tag{B5}$$

where, to the first order,

$$\left([G_p^o] + [g_p^i]\right)^{-1} \simeq [G_p^o]^{-1} - [G_p^o]^{-1}[g_p^i][G_p^o]^{-1} . \tag{B6}$$

Since $d\lambda^i$ is simply a scalar, define

$$\begin{bmatrix} e_p^i & \underline{f}_p^{i^T} \\ \underline{f}_p^i & [g_p^i] \end{bmatrix} = d\lambda^i \begin{bmatrix} e_p^o & \underline{f}_p^{o^T} \\ \underline{f}_p^o & [g_p^o] \end{bmatrix} . \tag{B7}$$

Thus, to the first order

$$\beta^i \simeq \frac{\lambda_p}{R\,\phi_p^2}\Big[\Big(E_p^o - \underline{F}_p^{oT}[G_p^o]^{-1}\underline{F}_p^o\Big) + d\lambda_i\Big(e_p^o$$

$$-\underline{F}_p^{oT}[G_p^o]^{-1}\underline{f}_p^o + \underline{F}_p^{oT}[G_p^o]^{-1}[g_p^o][G_p^o]^{-1}\underline{F}_p^o - \underline{f}_p^{oT}[G_p^o]^{-1}\underline{F}_p^o\Big) \quad (B8)$$

which readily gives Eq. (26).